AD-A144 783 DESIGN PROPOSALS FOR TORSIONAL BUCKLING OF STIFFENERS (U) MASSACHUSETTS INST OF TECH CAMBRIDGE DEPT OF OCEAN ENGINEERING S L COULTER MAY 84 N66314-70-A-0073 1/1

UNCLASSIFIED F/G 20/11 NL

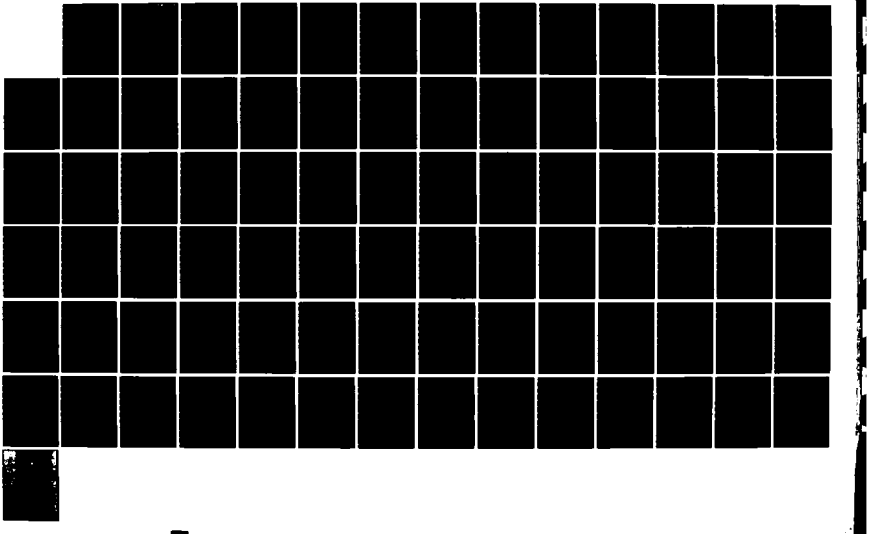

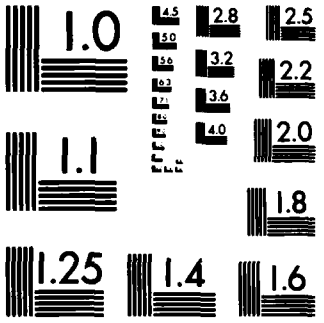


MICROCOPY RESOLUTION TEST CHART
NATIONAL BUREAU OF STANDARDS-1963-A

N66314-70-A-0023

# DESIGN PROPOSALS FOR TORSIONAL BUCKLING OF STIFFENERS

by

STEPHANIE LYNNE COULTER

B.A., Saint Francis College
(1974)

Submitted to the Department of
Ocean Engineering
in Partial Fulfillment of the
Requirements of the Degrees of

OCEAN ENGINEER

and

MASTER OF SCIENCE IN MECHANICAL ENGINEERING

at the



June 1984



Signature of Author: Stephanie Lynne Coulter
Department of Ocean Engineering
11 May 1984

Certified by: Paul C. Xirouchakis
Professor P.C. Xirouchakis
Thesis Supervisor

Certified by: David M. Parks
Professor D.M. Parks
Thesis Reader

Accepted by: W.M. Rohsenow
Professor W.M. Rohsenow
Chairman, Mechanical Engineering Departmental Committee

Accepted by: A. Douglas Carmichael
Professor A. D. Carmicheal
Chairman, Ocean Engineering Departmental Committee

# DESIGN PROPOSALS FOR TORSIONAL BUCKLING OF STIFFENERS

by

STEPHANIE LYNNE COULTER

Submitted to the Department of Ocean Engineering on May 11, 1984 in partial fulfillment of the requirements for the Degrees of Ocean Engineer and Master of Science in Mechanical Engineering.

## ABSTRACT

The ability to predict torsional instability in the early stages of design can have important consequences on the design of both conventional and high performance ships. This thesis develops fast approximate methods of torsional buckling analysis for particular application in the concept, feasibility, and preliminary stages of ship design.

Two simplified models of stiffeners commonly used in ship construction were presented. The first was an ideal I section stiffener. The second, a flat bar stiffener, which was included in this analysis because of its favorable productional properties and wide useage. These models, with initial imperfections, were subjected to axial compressive end loading and the resultant behavior analyzed. The approach of the analysis of this thesis was an application of the energy method to determine the critical buckling stress instead of the more commonly used equilibrium approach. Both beam theory and thin plate theory were used in energy-work relationships in these derivations. Then the first yield load was determined utilizing the Perry-Robertson approach. Integrated into all phases of this exploration was the concept of the geometric imperfections of the stiffeners.

Thesis Supervisor: Dr. P.C. Xirouchakis

Thesis Reader: Dr. D.M. Parks

ACKNOWLEDGEMENTS

The author wishes to express her appreciation to Professor P.C. Xirouchakis for his guidance, advice and unfailing encouragement which made this thesis possible. The author is especially grateful to Professor Xirouchakis for the generous sharing of his time throughout this undertaking.

The author would also like to thank Professor D.M. Parks for his words of encouragement and advice.

Finally, the author wishes to express her deeply felt thanks to her husband, Edward, for his patience, understanding and love.

TABLE OF CONTENTS



CHAPTERS

NOMENCLATURE

$A$ Nondimensional parameter

$a$ Length of stiffener between transverse supports

$b$ Uniform stiffener spacing

$b_e$ Plating effective width

$B$ Angle of rotation of the stiffener about the toe

$B^*$ Initial imperfection of the stiffener in terms of a rotation angle about the toe

$B_o$ Amplitude of the sinusoidal function for $B$

$B_o^*$ Amplitude of the sinusoidal function for $B^*$

$C$ Rotational spring constant (moment/length) of the supporting plating

$C_w$ Longitudinal warping constant of stiffener

$D$ Flexural rigidity of plating

$D_w$ Flexural rigidity of web plating of stiffener

$d$ Depth of flat bar stiffener; overall depth of Tee stiffener

$d_c$ Depth of stiffener to midthickness of flange

$d_w$ Depth of web

$E$ Young's Modulus of the material

$\varepsilon_x$ Membrane strain

$f_w$ Width of stiffener flange

G Shear Modulus of the material

h Height of neutral axis of plate-stiffener combination from midplane of plating

I Effective vertical moment of inertia of stiffener and associated effective width of plating

$I_p$ Polar moment of inertia of stiffener about toe

$I_t$ Vertical moment of inertia of stiffener alone about toe

$I_z$ Moment of inertia of stiffener about web plane

J St. Venant's torsion constant for stiffener

L Reduced slenderness ratio

M(x) Moment developed in the stiffener by the total torque

m Mode number

P Axial end load

s Height of stiffener shear center above toe

$\sigma_{CR}$ Elastic axial torsional buckling stress in stiffener (critical stress)

$\sigma_{CL}$ Elastic axial torsional buckling stress limit of stiffener (classical stress)

$\sigma_e$ Axial stress in stiffener

$\sigma_x$ Axial stress component

$(\sigma_x)_{MAXT}$ Maximum compressive stress developed by the torque

$\sigma_y$ Tensile yield stress of material

$T_o$ Amplitude of the sinsoidal torque function

T Total torque developed in the stiffener structure by the loading

$T_{SV}$ St. Venant's torque developed in the stiffener

$T_w$ Warping torque developed in the stiffener

t Plate thickness

$t_f$ Stiffener flange thickness

$t_w$ Stiffener web thickness

u Displacement in the longitudinal (x) direction

V Total strain energy of the structure

v Sideways flexure (y) of stiffener

$v^*$ Initial imperfection of stiffener in horizontal (y) direction

W Total work of the applied force

w Vertical flexure (z) of stiffener

$w^*$ Initial imperfection of the stiffener in the vertical (z) direction

z Height of stiffener centroid above toe

$\nu$ Poisson's Ratio

Note: x,y or z subscripts indicate partial derivatives with respect to those coordinates. These are used particularly with $v$, $v^*$, $w$, $w^*$, $B$, $B^*$.

## LIST OF FIGURES

## LIST OF TABLES

## INTRODUCTION

The subject of this thesis is to develop a simplified analytical method of predicting torsional buckling of stiffeners used in ship structures. Torsional buckling or instability is the phenomena by which a column, at a certain axial load, fails suddenly in a combined mode of twist and lateral bending of the cross section (reference 7). Figure (0-1a) (from reference 6) illustrates the failure mode referred to here as torsional buckling - in this case for a flat bar stiffener. Figure (0-1b) illustrates the failure mode of the tripping phenomenon which is not covered in this analysis. Figure (0-2) (reference 6) is the experimental load deflection curve for the failure of a flat bar stiffener under an axial load. Point A of the solid (experimental) curve of figure (0-2) is the ultimate strength load. As can be seen from figure (0-2), the curve proceeds in a downward fashion - the bar looses stiffness and fails from this point.

The ability to predict torsional instability in the early stages of design can have important consequences on the design of both conventional and high performance ships. It is the intention of this thesis to develop fast approximate methods of torsional

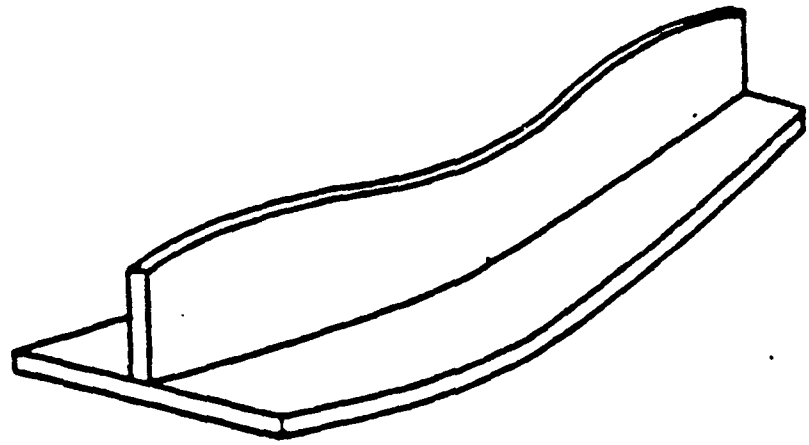

Figure (0-1a) Torsional Buckling

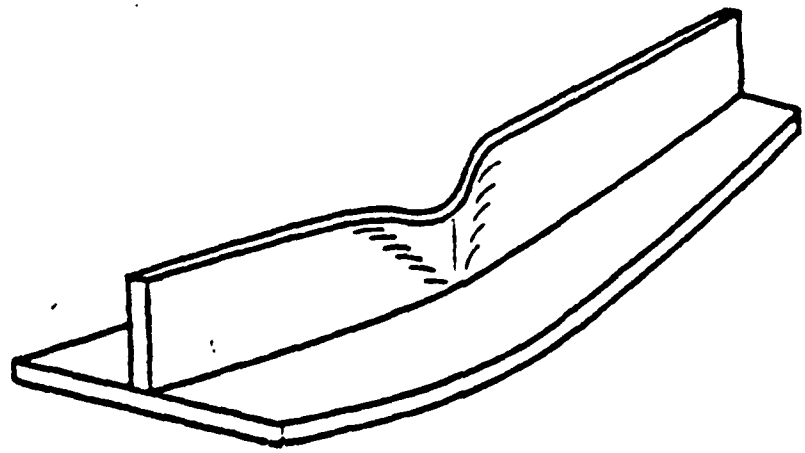

Figure (0-1b) Tripping

Figure (0-1) Characterization of Torsional Buckling and Tripping in a Flat Bar Stiffener

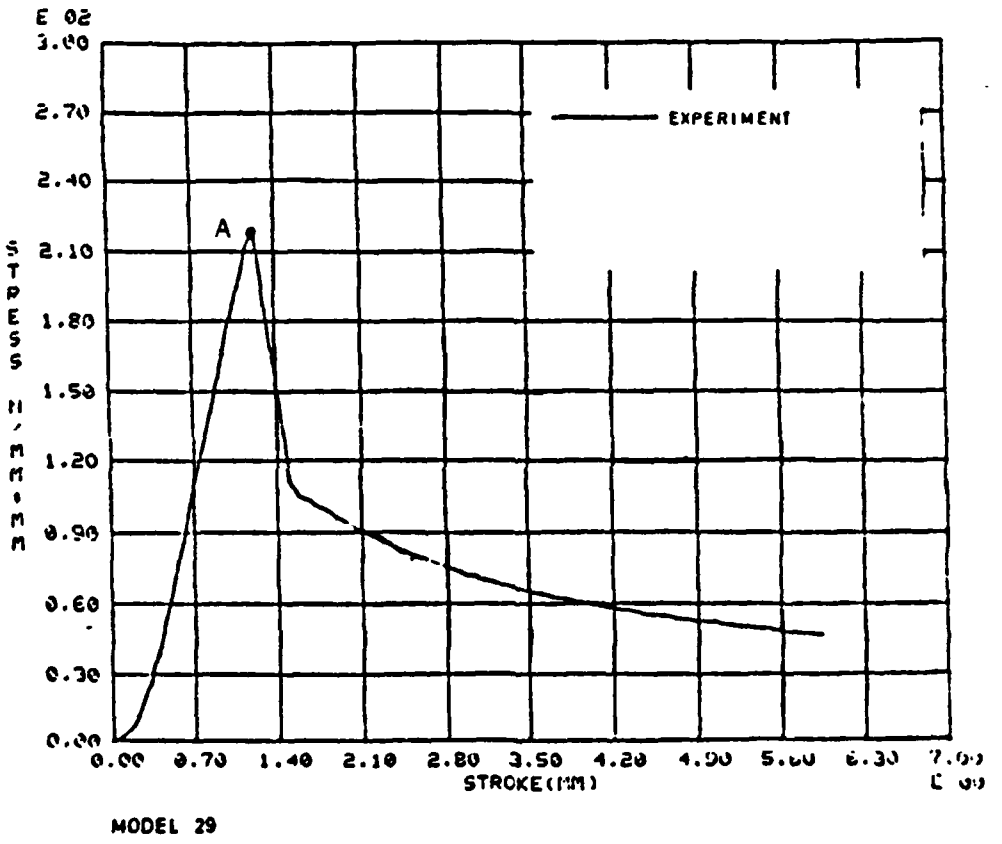


Figure (0-2) Experimental Load Deflection Curve

buckling analysis for particular application in the concept, feasibility, and preliminary stages of ship design.

To this end, two simplified models of stiffeners commonly used in ship construction will be presented. The first is an ideal I section stiffener. The second, a flat bar stiffener, which is included in this analysis because of its favorable productional properties and wide useage. These models, with initial imperfections, will be subjected to axial compressive end loading and the resultant behavior analyzed. The approach of the analysis of this thesis will be an application of energy methods to determine the critical buckling stress instead of the more commonly used equilibrium approach. Both beam theory and thin plate theory are used in energy-work relationships in these derivations. Then the first yield load is determined utilizing the Perry-Robertson approach as described in references (9,14). Integrated into all phases of this exploration will be the concept of the geometric imperfections of the stiffeners.

It is the intention of this thesis, using the above mentioned approach, to lay groundwork which would have the potential for future expansion to include mode interaction - to be able to easily analyze combined

loadings etc..

Particular emphasis is placed here upon inclusion of the geometrical initial deformities of the stiffeners which occur during the manufacture and through day to day usage of the ship. It is well known that these geometric imperfections can drastically reduce the strength of the structural member. But current design standards (references 10,11 etc) have not tried to quantify these values. Some design codes (example: reference 10) have specified tolerence limits of various geometric parameters which must be met before the design formulae are considered valid. Granted, in the concept, feasibility and preliminary stages of ship design where the ship only exists on paper, the designer would have no knowledge of the end resulting imperfections of the actual ship. Hopefully, in the future, with the advent of better production control in shipyards and the incursion of the computer into ship production facilities, this information will be collected and statistically analyzed.

In addition, once the ship is manufactured, these formulae will provide a quick and easy evaluation of the actual critical buckling stress in terms of physical parameters. Thus, this analysis has made a special effort to define the imperfections in easily

measured terms. This analysis measures the horizontal or vertical movement of the shear center of the stiffener at its point of greatest deflection and assumes a simple sinusoidal distribution. Knowledge of the web depth easily converts the imperfection into a rotational angle. Here, the stiffener is considered to rotate about its toe or base. In other words, the base plating is considered much larger and stiffer. Figure (0-3) illustrates this simplified concept for a Tee stiffener.

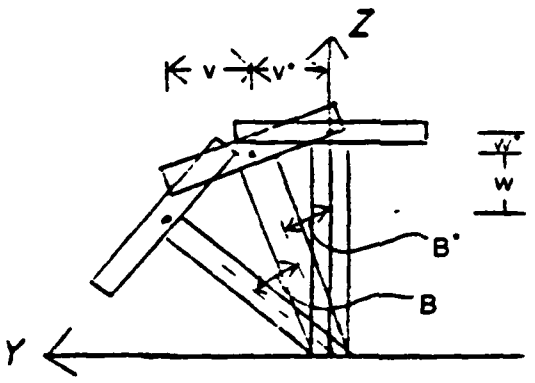


Figure (0-3) Tee Stiffener

Currently the method of handling the stiffener failure problem is incorporated into the use of factors of safety. But, with recent attempts to further optimize ship structures - in particular to minimize

the amount of weight of a ship that must be devoted to its structure - better, yet reliable, methods must be devised. Remember, with a ship, less weight in the structure equates to more weight for the payload be it weapons for a military ship or cargo for a civilian ship.

This thesis concludes with a comparison between the formulae derived from the simplified models presented here and published formulae, published finite element analysis, and experimentally derived results.

## 1. DESCRIPTION OF MODELS

Torsional buckling or instability is characterized by a twisting of the stiffener about its line of attachment to the plating. This deformation pattern involves both sideways and vertical flexure (v,w) and rotation (B) of the stiffener as shown in figure (1) as described in reference (3).

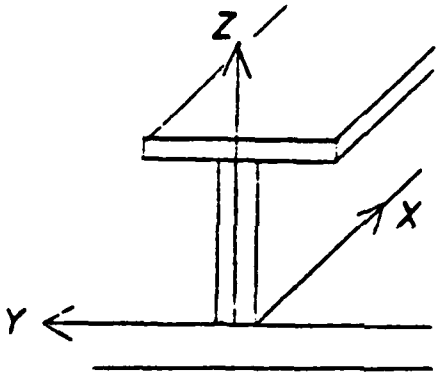


Figure (1-1a) Coordinate System

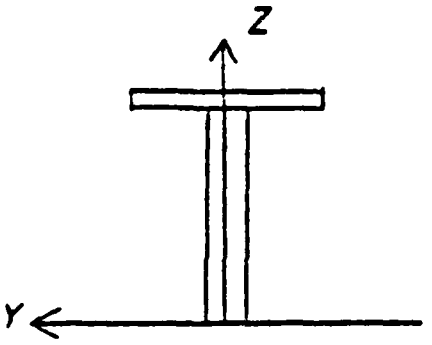


Figure (1-1b) Undeformed

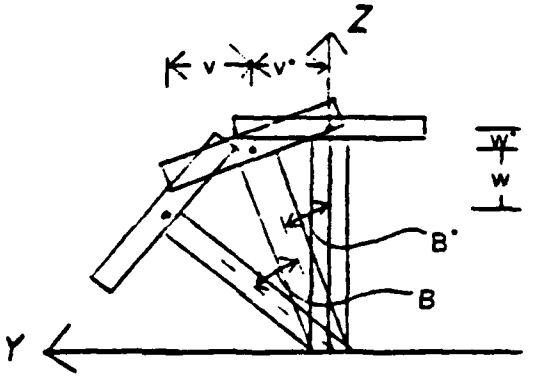


Figure (1-1c) Deformed

Figure (1-1) Characterization of Torsional Buckling

## 1.1 Model I.

The first model considered is a simplification of an ideal I-section. It consists of an I-beam with zero torsional rigidity. The web of the I-beam transmits only shear forces. In effect, it looks like two unequal flanges:

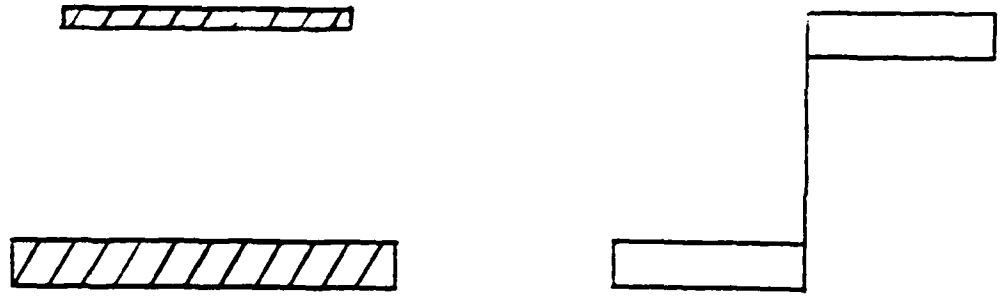

I-beam Stress Distribution

Figure (1-2) Model I

This model has been considered in reference (4). However, reference (4) used an equilibrium approach and initial imperfections were considered as an eccentricity of the axial load. The resulting equations of the critical stress were quite complicated.

Figure (1-3) illustrates the geometric parameters of this model.

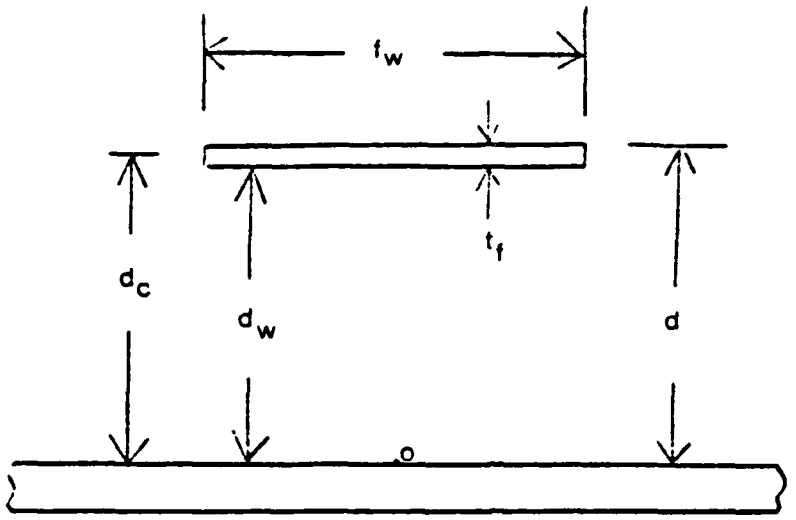


Figure (1-3) - Geometric Torsional Buckling Parameters for Model I

$I_z$ - Moment of inertia about the web plane (top flange only)

$$I_z = (t_f f_w^3)/12$$

s - Height of shear center above toe (origin) (top flange only)

$$s = d_c$$

$C_w$ - Longitudinal warping constant about shear center of stiffener alone (top flange only)

$$C_w = 0$$

$I_t$ - Vertical moment of inertia about toe (top flange only)

$$I_t = f_w t_f (d_c^2 + (1/12)t_f^2)$$

$I_p$ - Polar moment of inertia about toe

$$I_p = I_t + I_z$$

z - Height of centroid above toe

$$z = d_c$$

J - St. Venant's torsion constant (top flange only)

$$J = (f_w t_f^3)/3$$

## 1.2 Model II.

The second model considered is the simple flat bar stiffener illustrated in figure (1-4).

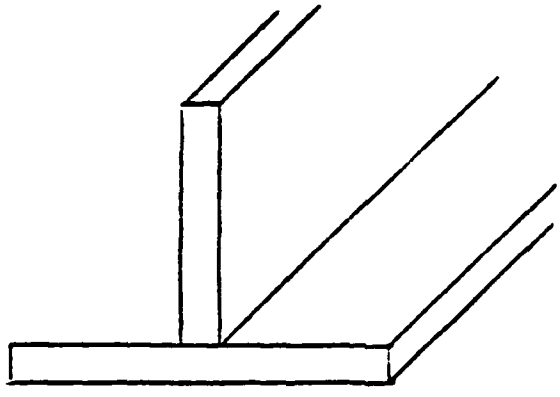

Figure (1-4) Model II - Flat bar stiffener.

Figure (1-5) illustrates the geometric parameters of this model.

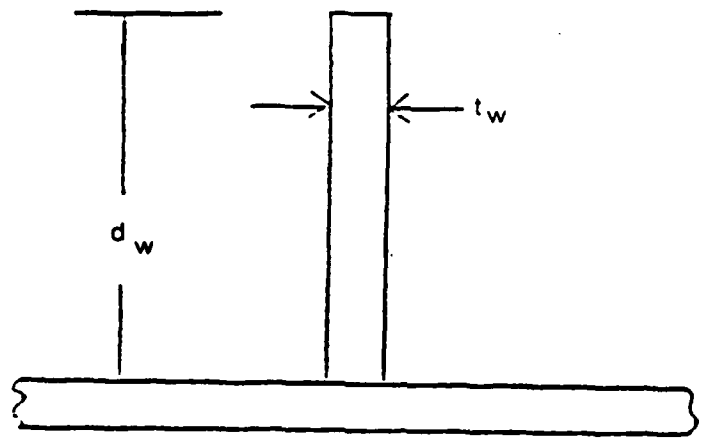


Figure (1-5) - Geometric Torsional Buckling Parameters for Model II

$I_z$ - Moment of inertia about the web plane (web only)

$$I_z = (d_w t_w^3)/12$$

s - Height of shear center above toe (origin) (web only)

$$s = d_w/2$$

$C_w$ - Longitudinal warping constant about shear center of stiffener alone

$$C_w = 0$$

$I_t$ - Vertical moment of inertia about toe (web only)

$$I_t = (t_w d_w^3)/3$$

$I_p$ - Polar moment of inertia about toe

$$I_p = I_t + I_z$$

z - Height of centroid above toe

$$z = d_w/2$$

J - St. Venant's torsion constant

$$J = (d_w t_w^3)/3$$

$D_w$ - Flexural rigidity of the web plate

$$D_w = \frac{Et_w^3}{12(1-\nu^2)}$$

## 2. MODEL I - TORSIONAL BUCKLING UNDER AXIAL LOADS

### 2.1 Development of the Strain Energy Equation.

Since Model I basically consists of two unequal flanges with the top flange rotating about the bottom flange, the torsional rigidity is considered only for the top flange. Thus the strain energy equation consists of three parts (reference 1). The first term represents sideways bending. The second term represents longitudinal warping. The third term represents the torsional rigidity of the top flange alone. The strain energy for a length a is:

$$V = 1/2 \int_0^a (EI_z v_{xx}^2 + EC_w B_{xx}^2 + GJB_x^2)dx$$

Also from geometrical properties we have (see figure 1-3):

$$v \approx sB$$

Thus:

$$V = 1/2 \int_0^a (EI_z s^2 B_{xx}^2 + EC_w B_{xx}^2 + GJB_x^2)\, dx$$

$$V = 1/2 \int_0^a [E(I_z s^2 + C_w)B_{xx}^2 + GJB_x^2]\, dx$$

The following choice of B is made, in order to meet certain boundary conditions (ie $B_{xx} = 0$ at x=0, x=a ) and to keep B simple.

$$B = B_o \sin (m\pi x/a)$$

Thus for Model I:

$$V = 1/4\ a\ B_o^2 (m\pi/a)^2 [\ E(I_z s^2 + C_w)(m\pi/a)^2 + GJ\ ]$$

## 2.2 Sign Convention

Before development of the virtual work equation, a note should be said about the sign convention used here. Compression is held to be a positive stress and tension as negative. The following figures illustrate the sign convention used here.

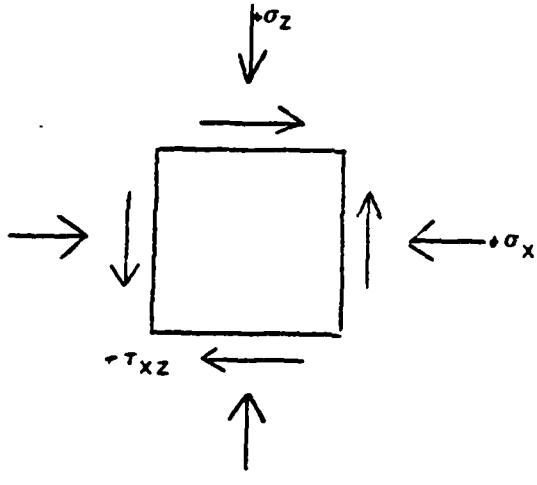


Figure (2-1) Sign convention for inplane axial and shear stress components.

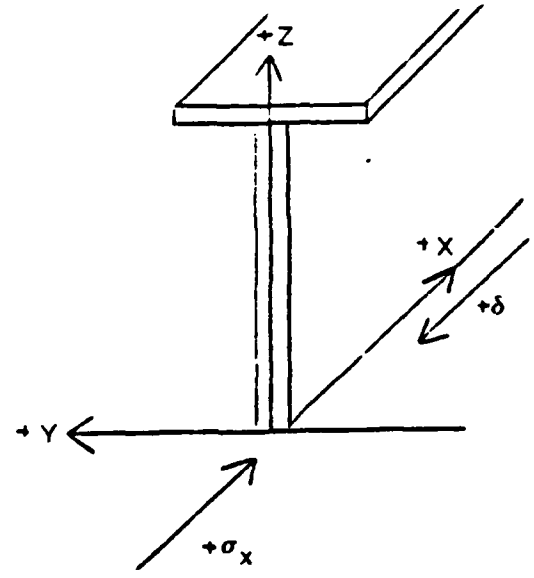


Figure (2-2) Application of sign convention for case of an axial load.

## 2.3 Development of Virtual Work Equation.

Model I is not assumed to be perfect but rather to have initial imperfections. These initial imperfections $v^*$, $w^*$ and $\beta^*$ and the additional deformations v, w and $\beta$ are illustrated in figure (2-3).

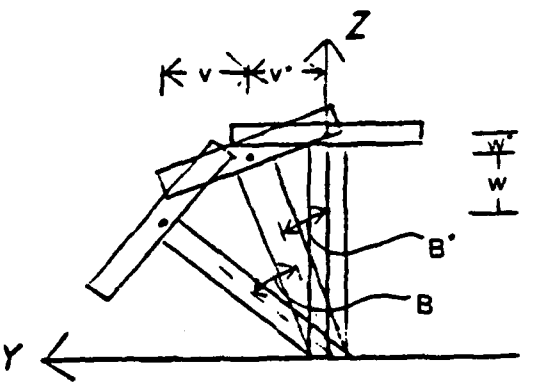


Figure (2-3) Illustration of initial imperfections v*, w*, B* and additional deformations v, w, B.

The virtual work for the case of an inplane axial load becomes (reference 1):

$$W = \iint_A \varepsilon_x \, u(y,z) \, dy \, dz$$

Thus using figure (1-1), it can be shown that the strain of the centroidal axis in the bent configuration, $\varepsilon_x$ (membrane strain), is (reference 1):

$$\varepsilon_x = -u_x + 1/2(v_x)^2 + 1/2(w_x)^2$$

for a perfect I section. With imperfections, we substitute:

$$v + v^{*} \quad \text{for } v$$

$$w + w^{*} \quad \text{for } w$$

Thus:

$$\varepsilon_x = -u_x + 1/2(v_x + v_x^{*})^2 + 1/2(w_x + w_x^{*})^2$$

using the inextensibility assumptions, set:

$$\varepsilon_x = 0$$

we have:

$$u_x = 1/2(v_x + v_x^{*})^2 + 1/2(w_x + w_x^{*})^2$$

$$u = 1/2 \int_0^a [(v_x + v_x^{*})^2 + (w_x + w_x^{*})^2] \, dx$$

where $u = u(y,z)$.

From geometrical relationships (see figure (2-3))

$$v \cong zB \qquad w \cong -yB$$

$$v^{*} \cong zB \qquad w^{*} \cong -yB$$

(2-1)

$$v_x \cong zB \qquad w_x \cong -yB$$

$$v_x^{*} \cong zB \qquad w_x^{*} \cong -yB$$

Substituting and integrating we get:

$$u(y,z) = 1/2 \int_0^a (z^2 B_x^2 + 2z^2 B_x B_x^* + z^2 B_x^{*2}$$

$$+ y^2 B_x^2 + 2y^2 B_x B_x^* + y^2 B_x^{*2}) \, dx$$

$$u(y,z) = 1/2 \int_0^a (z^2 + y^2)(B_x + B_x^*)^2 \, dx$$

Again using the simple choice for B and $B^*$:

$$B = B_o \sin(m\pi x/a)$$

$$B^* = B_o^* \sin(m\pi x/a)$$

Thus:

$$u(y,z) = 1/2 \int_0^a (z^2 + y^2)[(m\pi/a)B_o \cos(m\pi x/a)$$

$$+ ((m\pi/a)B_o^* \cos(m\pi x/a)]^2 \, dx$$

$$u(y,z) = 1/2 \int_0^a (z^2 + y^2)(B_o + B_o^*)^2$$

$$* [(m\pi/a)\cos(m\pi x/a)]^2 \, dx$$

$$u(y,z) = 1/2(z^2 + y^2)(B_o + B_o^*)^2 (m\pi/a)^2$$

$$* [x/2 + (\sin(2m\pi x/a)/(4m\pi/a)]_0^a$$

$$u(y,z) = 1/4(z^2+y^2)(B_o+B_o^*)^2(m\pi/a)^2 a$$

The work equation now becomes:

$$W = \iint_A \sigma_x [1/4(z^2+y^2)(B_o+B_o^*)^2(m\pi/a)^2 a]\, dy\, dz$$

For the current situation of end loading, $\sigma_x = \sigma_e$

$$W = \sigma_e [1/4(B_o+B_o^*)^2(m\pi/a)^2 a] \iint_A (z^2+y^2)\, dy\, dz$$

But note that:

$$\iint_A (z^2 + y^2)\, dy\, dz = I_p$$

Thus:

$$W = 1/4\, \sigma_e (B_o+B_o^*)^2(m\pi/a)^2 a\, I_p$$

## 2.4 Determination of the Critical Buckling Stress.

Applying the calculus of variations with respect to $B_o$ to the work and strain energy equations yields (reference 5):

$$\delta W = 1/2 \, \sigma_e (B_o + B_o^*)^2 (m\pi/a)^2 a I_p \delta B_o$$

$$\delta V = 1/2 \, a B_o (m\pi/a)^2 [E(I_z s^2 + C_w)(m\pi/a)^2 + GJ] \delta B_o$$

Applying the principle of minimum potential energy:

$$\Pi = \delta V - \delta W = 0$$

we get:

$$\delta W = \delta V$$

Solving for $\sigma_e$:

$$\sigma_e = \frac{[E(I_z s^2 + C_w)(m\pi/a)^2 + GJ]}{I_p} \frac{B_o}{B_o + B_o^*} \qquad (2\text{-}2)$$

It can be seen by inspection that the lowest buckling stress occurs for one wave, m = 1, since m must be an integer. Thus:

$$\%_e = \%_{CR}$$

As it can easily be seen, as $B_o$ becomes large $\%_{CR}$ approaches the limit of:

$$\%_{CL} = \frac{[E(I_z s^2 + C_w)(m\pi/a)^2 + GJ]}{I_p} \qquad (2\text{-}3)$$

Figure (2-4) illustrates the behavior of $\%_{CR}$ with increasing $B_o + B_o^*$.

Further simplification and rearranging of equations (2-2) and (2-3) provides:

$$\%_{CR} = \%_{CL} \frac{B_o}{B_o + B_o^*}$$

$$\%_{CR\,o} B_o + \%_{CR\,o} B_o^* = \%_{CR\,o} B_o$$

$$B_o = \frac{B_o^*}{\%_{CL}/\%_{CR} - 1} \qquad (2\text{-}4)$$

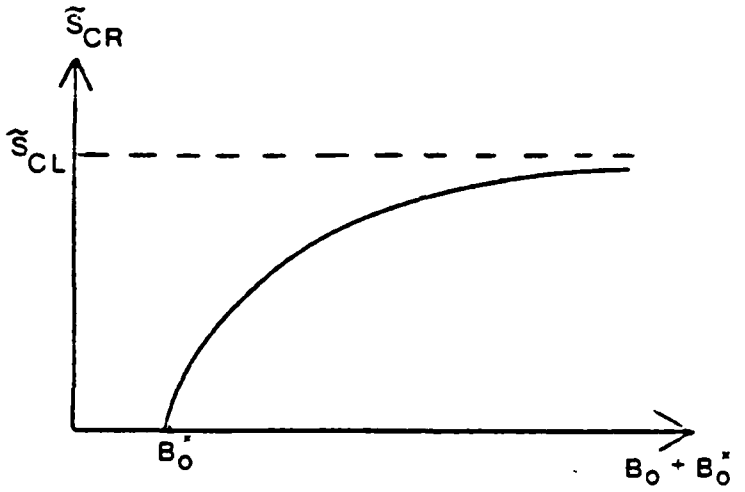


Figure (2-4) $\tilde{S}_{CR}$ vs. $(B_o + B_o^*)$

## 2.5 Determination of the First Yield Load.

To determine the first yield load, the total torque developed in the torsional buckling process must be first evaluated. This torque will consist of two parts. The first term consists of the well known St. Venant's Torque (reference 1). The second term represents the warping torque (reference 2).

From reference (1):

$$T = T_{SV} + T_{W}$$

where:

$$T_{SV} = GJB_{x}$$

and from reference (2):

$$T_{W} = - EI_{z} \, c \, d^{3} w / dx^{3}$$

and from geometry;

$$w_{x} = c \, B_{x}$$

resulting in:

$$T_{W} = - EI_{z} \, c \, d^{2} B / dx^{3}$$

Thus the total torque is:

$$T = GJB_x - EI_z d^2 B_{c\,xxx} \qquad (2\text{-}5)$$

Figure (2-3) illustrates the above equations.

Again a simple choice of B is made, and with m = 1:

$$B = B_o \sin(\pi x/a) \qquad (2\text{-}6)$$

Equation (2-5) now becomes:

$$T = GJ(\pi/a)B_o \cos(\pi x/a) + EI_z d^2_c (\pi/a)^3 B_o \cos(\pi x/a)$$

$$T = (\pi/a)B_o \cos(\pi x/a)[GJ + EI_z d^2_c (\pi/a)^2]$$

Choosing a simple sinusoidal shape for T allows:

$$T = T_o \cos(\pi x/a)$$

Thus:

$$T_o = (\pi/a)B_o [GJ + EI_z d^2_c (\pi/a)^2] \qquad (2\text{-}7)$$

To eliminate $B_o$, equation (2-4) is applied to equation (2-7).

$$T_o = [GJ + EI_z d^2_c (\pi/a)^2](\pi/a) \frac{B_o^*}{(\%_{CL}/\%_{CR} - 1)} \qquad (2\text{-}8)$$

From sectional considerations, an evaluation of the maximum stress can be made.

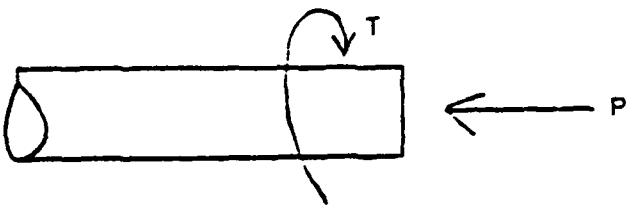


Figure (2-5) Sectional illustration.

The moment developed by the torque in terms of deflections is (reference 2):

$$M(x) = - EI_z w_{xx}$$

So the maximum compressive stress developed in the flange due to the torque is:

$$(\sigma_x)_{MAXT} = \frac{- EI_z d_B f_c w_{xx}}{2I_z}$$

$$(\sigma_x)_{MAXT} = - Ed_B f_c w_{xx} /2$$

Application of the above definition for B (equation 2-4) leaves:

$$(\sigma_x)_{x\ MAXT} = \frac{E d_c f_w}{2} (\pi/a)^2 B_o \sin(\pi x/a)$$

A choice of x is made such that $(\sigma_x)_{x\ MAXT}$ is a maximum:

$$(\sigma_x)_{x\ MAXT} = \frac{E d_c f_w}{2} (\pi/a)^2 B_o \qquad (2\text{-}9)$$

Equations (2-7) and (2-9) are combined to eliminate $B_o$.

$$(\sigma_x)_{x\ MAXT} = \frac{E d_c f_w T_o (\pi/a)^2}{2[GJ_z + EI_c (\pi/a)^2]} \qquad (2\text{-}10)$$

Using equation (2-8) leads to:

$$(\sigma_x)_{x\ MAXT} = \frac{E d_c f_w (\pi/a)^2}{2} \frac{B_o^*}{[\sigma_{CL}/\sigma_{CR} - 1]} \qquad (2\text{-}11)$$

Note that when $B_o^* = 0$ that this equation leads to an indeterminate form of $\sigma_x$ since $\sigma_{CL} = \sigma_{CR}$.

The total maximum stress can now be described by:

$$(\sigma_x)_{x\ TOTAL} = (\sigma_x)_{x\ MAXT} + P/A$$

where

$$P/A = \sigma_{CR}$$

Thus the yield stress has been shown to be:

$$\sigma_y = (\sigma_y)_{x\ MAXT} + \sigma_{CR} \qquad (2\text{-}12)$$

Using equation (2-11) in equation (2-12):

$$\sigma_y = \frac{E d_c f_w^2 (\pi/a)^2}{2} \cdot \frac{B^*}{\sigma_{CL}/\sigma_{CR} - 1} + \sigma_{CR} \qquad (2\text{-}13)$$

Solving for $\sigma_{CR}$ and dividing by $\sigma_y^2$ to place into nondimensional form yields:

$$\left(\frac{\sigma_{CR}}{\sigma_y}\right)^2 - \left(1 + \frac{\sigma_{CL}}{\sigma_y} + \frac{E d_c f_w^2 (\pi/a)^2 B_o^*}{2\sigma_y}\right)\left(\frac{\sigma_{CR}}{\sigma_y}\right) + \left(\frac{\sigma_{CL}}{\sigma_y}\right) = 0 \qquad (2\text{-}14)$$

Choosing the smallest root and simplifying the equation by introducing a slenderness ratio L:

$$L = \sqrt{\frac{\sigma_y}{\sigma_{CL}}} \qquad (2\text{-}15)$$

and letting:

$$A = \frac{(\pi/a)^2 E d_c f_w B_o^*}{2\sigma_y} \qquad (2\text{-}16)$$

Then :

$$\frac{\sigma_{CR}}{\sigma_y} = \frac{(1 + 1/L^2 + A) - \sqrt{(1 + 1/L^2 + A)^2 - 4/L^2}}{2} \qquad (2\text{-}17)$$

A plot of $\sigma_{CR}/\sigma_y$ vs L for various values of A is shown in figure (2-6). Figure (2-6) was compared with various design criteria from reference (10) and it was found that equation (2-17) was similar to design equations of reference (10). However, the reduced slenderness ratio, L, of reference (10) is based upon simple Euler buckling and the geometric parameter, A, is of course different. The column curves of reference (10) were quite similar in appearance and range of values to that found in figure (2-6).

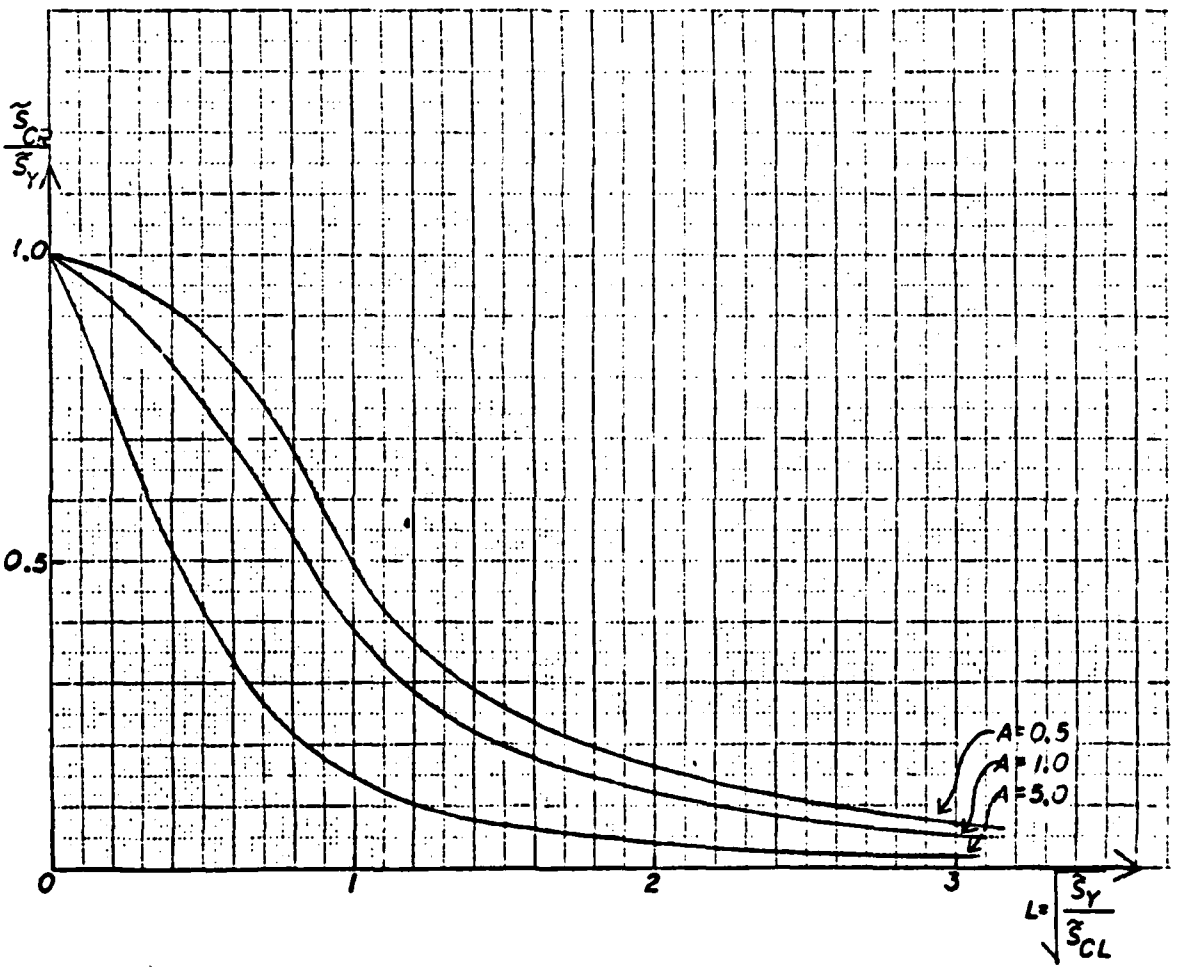


Figure (2-6) Column Curves

## 3. MODEL II - TORSIONAL BUCKLING UNDER AXIAL LOADS

### 3.1 Development of the Strain Energy Equation.

Since Model II is the very simple case of a flat bar stiffener, thin plate theory can be easily utilized in the development of the strain energy equation. Much of this section has been patterned after a similar analysis presented in reference (3).

For a web plate of uniform thickness and a length a the strain energy is repensented by (reference 5):

$$V = 1/2\, D_w \int_o^a \int_o^{d(x)} [(v_{xx} + v_{zz})^2 - 2(1-\nu)[v_{xx} v_{zz} - v_{xz}^2]]\, dx\, dz + 1/2 \int_o^a CB^2\, dx$$

The second term represents the rotation of the supporting plate structure modeled here as an elastic spring. $D_w$ is the flexural rigidity of the web plate. From geometrical considerations:

$$v = zB$$

making a simple choice for B;

$$B = B_o \sin (m\pi x/a)$$

substituting into the expression for the strain energy and integrating over a constant depth d results in:

$$V = D_w a d (m\pi/a)^2 B_o^2 [ d^2 (m\pi/a)^2 + 6(1 - \nu) ]/12 + CB_o^2 a/4 \qquad (3-1)$$

3.2 Development of the Virtual Work Equation.

As for Model I, Model II is not assumed to be perfect but rather to have initial imperfections. These initial imperfections $v^*$, $w^*$, $B^*$ and the additional deformations v, w, and B are illustrated in figure (3-1).

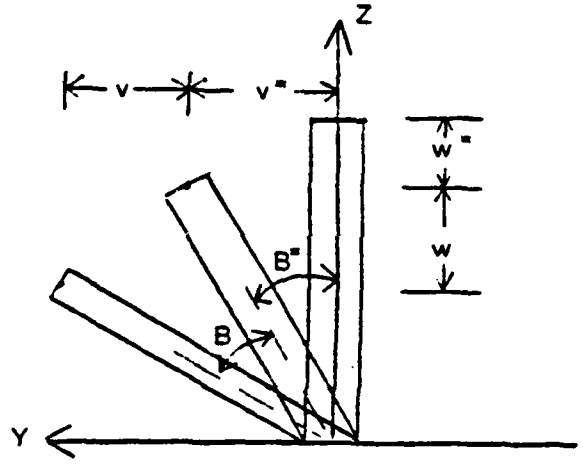


Figure (3-1) Illustration of the initial imperfections v*, w*, B* and additional deformations v, w, B.

For the case of an inplane axial load, the work equation is :

$$W = \iint_A \sigma_x u(y,z)\, dy\, dz$$

From figure (3-1), it can be shown that :

$$\varepsilon_x = -u_x + 1/2(v_x)^2 + 1/2(w_x)^2$$

for a perfect web section. With imperfections, and using the inextensibility assumption with regard to the length of the stiffener setting $\varepsilon_x = 0$, the result is :

$$u_x = 1/2\,(v_x + v_x^*)^2 + 1/2(w_x + w_x^*)^2$$

$$u = 1/2 \int_o^a [(v_x + v_x^*)^2 + 1/2(w_x + w_x^*)^2]\, dx \qquad (3\text{-}2)$$

where $u = u(y,z)$

As shown in figure (3-1), the geometrical relationships (equations 2-1) are used to simplify equation (3-2):

$$u(y,z) = 1/2 \int_o^a (z^2 + y^2)(B + B^*)\, dx$$

A simple choice is made for B and $B^*$.

$$B = B_o \sin (m\pi x/a)$$

$$B^* = B_o^* \sin (m\pi x/a)$$

Thus:

$$u(y,z) = 1/4(z^2 + y^2)(B_o + B_o^*)(m\pi/a)^2 a$$

The work equation now becomes:

$$W = \iint_A \varepsilon_x [1/4(z^2 + y^2)(B_o + B_o^*)(m\pi/a)^2 a]\, dy\, dz$$

$$W = 1/4\ \sigma_x (B_o + B_o^*)^2 (m\pi/a)^2 a I_p$$

### 3.3 Determination of the Critical Buckling Stress.

Applying the calculus of variations with respect to $B_o$ to the work and strain energy equations yields:

$$\delta W = 1/2\ \sigma_x (B_o + B_o^*)^2 (m\pi/a)^2 a I_p \delta B_o$$

$$\delta V = \{ D_w a d (m\pi/a)^2 B_o [ d^2 (m\pi/a)^2 + 6(1 - \nu) ]/6 + C B_o^2 a/2 \} \delta B_o$$

Applying the principle of minimum potential energy:

$$\Pi = \delta V - \delta W = 0$$

$$\delta W = \delta V$$

Solving for $\sigma_e = \sigma_{CR}$:

$$\sigma_{CR} = \frac{D_w d (m\pi/a)^2 [d^2 (m\pi/a)^2 + 6(1-\nu)]/3 + C}{(m\pi/a)^2 I_p} \frac{B_o}{B_o + B_o^*} \qquad (3\text{-}3)$$

For the case of zero restraint against rotation; $C = 0$:

$$\zeta_{CR} = \frac{D_w d(m\pi/a)^2 [d^2(m\pi/a)^2 + 6(1-\nu)]}{3 I_p} \cdot \frac{B_o}{B_o + B_o^*} \qquad (3-4)$$

It is easily seen that the lowest $\zeta_{CR}$ for this case results from the simplest of mode shapes, m=1.

When the rotational restraint is not equal to zero; the lowest value of $\zeta_{CR}$ depends upon the degree of rotational restraint:

$$m = (a/\pi)(3C/D_w d^3)^{1/4} \qquad (3-5)$$

With the use of equation (3-5), m may be evaluated and rounded up or down to the nearest integer for the correct wave shape.

It is easily seen that as $B_o$ becomes large $\zeta_{CR}$ approaches a limit. Thus with $(\zeta_{CR})_{LIMIT} = \zeta_{CL}$ :

$$\zeta_{CL} = \frac{D_w d(m\pi/a)^2 [d^2(m\pi/a)^2 + 6(1-\nu)]/3 + C}{(m\pi/a)^2 I_p} \qquad (3-6)$$

Figure (3-2) illustrates the behavior of $\zeta_{CR}$ with increasing $B_o + B_o^*$.

Further simplification and rearranging of

equations (3-3) and (3-6) provides:

$$B_o = \frac{B_o^*}{\%_{CL}/\%_{CR} - 1} \qquad (3\text{-}7)$$

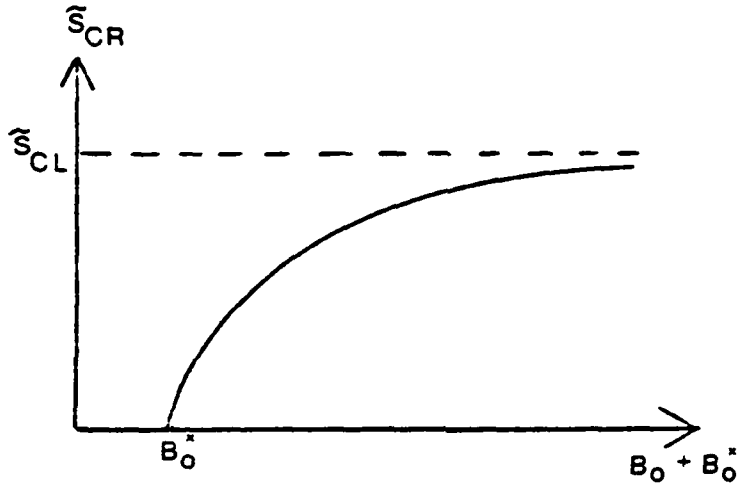


Figure (3-2) Behavior of $\%_{CR}$ with $B_o + B_o^*$

The first yield load will not be determined for this case under this method of analysis due to the relative complexity of equation (3-3) and due to the fact that the Perry-Robertson method will not lend itself to further simplification along this train of analysis. Since a simplified formula for design purposes is the goal of this thesis, the next chapter will use a different tactic to solve the problem.

# 4. MODEL II - GENERALIZED ANALYSIS

## 4.1 Method of Approach and Strain Energy Equation.

The analysis thus far for the case of a flat bar stiffener under end loading has proceeded along the lines of thin plate theory up to the development of an expression for the critical buckling stress.

This chapter uses beam theory to develop a simpler formulation in a manner analagous to that performed on Model I in chapter 2. In fact, this analysis will merely be a generalization of the results for Model I applied to Model II. It must be remembered here that Model I consisted of two unequal flanges with the top flange deforming or rotating about the bottom flange. At no time in the derivation of the formula for the critical stress of the tee stiffener is there an assumption made about the position of the top flange relative to the bottom flange. Thus the same analysis with minor changes will be performed for the flat bar stiffener. However, in the case of the flat bar stiffener of Model II, there is a restraining effect provided by the juncture of the flat bar with the plate. This in effect can be modeled as a spring with a rotational constant C. Thus the strain energy equation would have four terms (instead of the three terms for

Model I). These terms represent (in order of appearance) sideways bending; longitudinal warping; torsion; and rotation of the supporting plate structure modeled as an elastic spring. Thus the strain energy equation is:

$$V = 1/2 \int_0^a [EI_z v_{xx}^2 + EC_w B_{xx}^2 + GJB_x^2 + CB^2] \, dx$$

Again choose:

$$B = B_o \sin(m\pi x/a)$$

Substituting and integrating results in:

$$V = 1/4 \, a B_o^2 [ E(I_z s^2 + C_w)(m\pi/a)^4 + GJ(m\pi/a)^2 + C ]$$

Applying the calculus of variations with respect to $B_o$ yields:

$$\delta V = 1/2 \, a B_o [ E(I_z s^2 + C_w)(m\pi/a)^4 + GJ(m\pi/a)^2 + C ] \delta B_o \qquad (4\text{-}1)$$

## 4.2 The Work Equation.

The assumptions used in deriving the work equation for Model I are the same as for Model II. Thus from chapter 2 we have:

$$W = 1/4 \, \omega_e^2 (B_o^* + B_o)^2 (m\pi/a)^2 a I_p$$

and

$$\delta W = 1/2\ \sigma_e\ (B_o + B^*_o)(m\pi/a)^2\ a\ I_p\ \delta B_o \qquad (4\text{-}2)$$

## 4.3 Determination of the Critical Buckling Stress

Using equations (4-1) and (4-2) and applying the principle of minimum potential energy and solving for the stress yields (with $\sigma_e = \sigma_{CR}$):

$$\sigma_{CR} = \frac{E(I_z s_w^2 + C_w)(m\pi/a)^4 + GJ(m\pi/a)^2 + C_o}{(m\pi/a)^2\ I_p} \cdot \frac{B_o}{B_o + B^*_o} \qquad (4\text{-}3)$$

Let:

$$\sigma_{CL} = \frac{E(I_z s_w^2 + C_w)(m\pi/a)^4 + GJ(m\pi/a)^2 + C_o}{(m\pi/a)^2\ I_p} \qquad (4\text{-}4)$$

Using (4-4) in equation (4-3) and solving for $B_o$ yields:

$$B_o = \frac{B^*_o}{\sigma_{CL}/\sigma_{CR} - 1} \qquad (4\text{-}5)$$

Comparison of equation (4-3) with equation (2-1)

reveals the only difference is that equation (4-3) has an additional term in the numerator (specifically the spring constant C).

Since it is very difficult to quantify the spring constant C and (hopefully) since its value is small in comparison to other terms in expression (4-3), C will be set to zero value and ignored for the remainder of this analysis.

Thus for the case of C = 0, equation (4-3) reduces to equation (2-2).

## 4.4 Determination of the First Yield Load.

The determination of first yield load for the generalized case proceeds in a similar fashion as for the case of Model I.

Again the total torque consists of two parts (reference 1), St. Venant's torque and a warping torque. However, in this case the warping torque is (reference 2):

$$T_w = -EI_z \, d^3 w_x / dx^3$$

and

$$w_x = dB_x$$

resulting in:

$$T_w = -EI_z \frac{d^2}{dx^2} B_{xxx}$$

Thus the total torque is:

$$T = GJ_x B - EI_z \frac{d^2}{dx^2} B_{xxx}$$

Choosing B and T:

$$B = B_o \sin(m\pi x/a)$$

$$T = T_o \cos(m\pi x/a)$$

Leaves:

$$T_o = (\pi/a)[GJ + EI_z (\pi/a)^2 \frac{d^2}{dx^2}] B_o \qquad (4-6)$$

Using equation (4-5) to eliminate $B_o$ leaves:

$$T_o = (\pi/a)[GJ + EI_z (\pi/a)^2 \frac{d^2}{dx^2}] \frac{B^*_o}{(\sigma_{CL}/\sigma_{CR} - 1)} \qquad (4-7)$$

Again sectional considerations can be used to evaluate the maximum stress. The maximum stress developed in the stiffener due to the torque is now:

$$(\sigma_x)_{MAXT} = -Ed^2 B_{xx}$$

Application of the above definition of B and a choice of x such that $(\sigma_x)_{x\ MAXT}$ is a maximum leaves:

$$(\sigma_x)_{x\ MAXT} = Ed^2 (\pi/a)^2 B_o$$

Using equation (4-6) to eliminate $B_o$:

$$(\sigma_x)_{x\,MAXT} = \frac{Ed^2 T_o (\pi/a)^2}{[GJ + EI_z d^2 (\pi/a)^2]} \qquad (4\text{-}8)$$

Using equation (4-7) in equation (4-8) leads to:

$$(\sigma_x)_{x\,MAXT} = Ed^2 (\pi/a)^2 \frac{B_o^*}{(\sigma_{CL}/\sigma_{CR} - 1)} \qquad (4\text{-}9)$$

Again, from sectional considerations, the total maximum stress can be described by:

$$\sigma_y = (\sigma_x)_{x\,MAXT} + \sigma_{CR} \qquad (4\text{-}10)$$

Using equation (4-9) in equation (4-10), solving for $\sigma_{CR}$ and dividing by $\sigma_y^2$ to place into nondimensional form yields:

$$\left(\frac{\sigma_{CR}}{\sigma_y}\right)^2 - \left(1 + \frac{\sigma_{CL}}{\sigma_y} + \frac{Ed^2 (\pi/a)^2 B_o^*}{\sigma_y}\right)\left(\frac{\sigma_{CR}}{\sigma_y}\right) + \left(\frac{\sigma_{CL}}{\sigma_y}\right) = 0 \qquad (4\text{-}11)$$

Choosing the smallest root and simplifying the equation by the use of the reduced slenderness ratio (equation 2-15) but redefining parameter A as:

$$A = \frac{(\pi/a)^2 E d^2 B_o^*}{\sigma_y} \qquad (4\text{-}12)$$

Results in (equation 2-17):

$$\frac{\sigma_{CR}}{\sigma_y} = \frac{(1 + 1/L^2 + A) - \sqrt{(1 + 1/L^2 + A)^2 - 4/L^2}}{2} \qquad (4\text{-}13)$$

# 5. COMPARISONS WITH OTHER STUDIES.

## 5.1 Comparison between Thin Plate and Beam Theory Results

In chapter 3, the critical buckling stress of a flat bar stiffener was derived through the use of thin plate theory:

$$\sigma_{CR} = \frac{D_w \, d(m\pi/a)^2 \left[ d^2 (m\pi/a)^2 + 6(1-\nu) \right]/3 + C_{B_o}}{(m\pi/a)^2 \, I_p \left( B_o + B_o^* \right)}$$

(3-3)

In chapter 4, the critical buckling stress of a flat bar stiffener was found using one dimensional beam theory:

$$\sigma_{CR} = \frac{E(I_z s^2 + C_w)(m\pi/a)^4 + GJ(m\pi/a)^2 + C_{B_o}}{(m\pi/a)^2 \, I_p \left( B_o + B_o^* \right)}$$

(4-3)

It should be noted here that when:

$$D_w\, d^2(m\pi/a)^2\,[d^2(m\pi/a)^2 + 6(1-\nu)]/3 = E(I_z s^2 + C_w)(m\pi/a)^4 + GJ(m\pi/a)^2$$

the agreement between the two methods would be exact.

For the elastic range of experimentation and with:

$$D_w = \frac{Et_w^3}{12(1-\nu)} \qquad G = E/2(1+\nu) = E/2.6$$

$$I_z = (d_w t_w^3)/12 \qquad J = (d_w t_w^3)/3$$

$$d = d_w \qquad \nu = 0.3$$

The above relationship reduces to:

$$\frac{d_w^2(m\pi/a)^2}{10.92} + \frac{1}{2.6} \stackrel{?}{=} \frac{d^2(m\pi/a)^2}{12} + \frac{1}{7.8}$$

(Thin Plate Theory) (Beam Theory)

From a cursory examination it would appear that the Thin Plate Theory results (equation 3-3) will probably give a larger value for the buckling stress for the normal range of stiffener dimensions used in ships. To test this hypothesis, the dimensions of a flat bar

stiffener used in experiment #21 of reference (6) will be used.

where:

$d_w = 87.4$ cm

$a = 730$ cm

$m = 1$

For the thin plate theory:

$$\frac{d_w^2 (m\pi/a)^2}{10.92} + \frac{1}{2.6} = 0.398$$

For the beam theory:

$$\frac{d_w^2 (m\pi/a)^2}{12} + \frac{1}{7.8} = 0.14$$

Thus, within the elastic range, the thin plate theory results would indeed provide higher buckling stress. The beam thoery results may thus be too conservative. However, section 5.3 shows good agreement between equation (4-11) (first yield load) and experimental yield results.

## 5.2 Comparisons with Published Formulae.

Reference (3) performed a similar analysis to that performed in this thesis but without the inclusion of initial geometric imperfections.

For the case of a Tee stiffener subjected to an axial load, equation 21 of reference (3) allows (in the notation of this thesis):

$$\sigma_{CR} = \frac{GJ + E(I_z s^2 + C_w)(m\pi/a)^2 + C(a/m\pi)^2}{I_p}$$

Equation (2-2) of this thesis, for a Tee stiffener in an analysis which ignores the contribution of the web and includes the contributions of initial defects, is:

$$\sigma_{CR} = \frac{[E(I_z s^2 + C_w)(m\pi/a)^2 + GJ]}{I_p} \frac{B_o}{B_o + B_o^*}$$

Thus equation (2-2), for the case of an initially perfect Tee stiffener reduces to equation 21 of reference (3) when the rotational restraint is held to

be zero. However, it must be noted that since the physical models of the two derivations were slightly different - namely that the model used in this analysis consisted of two unequal flanges - some of the parameters of the equations will have different values (ie. $I_z$, J etc.).

For the case of a flat bar stiffener, equation 22 of reference (3) has:

$$\frac{\sigma_{CR}}{} = \frac{D_w d[(m\pi/a)^2 d^2 + 6(1-\nu)]}{3I_p} + \frac{C(a/m\pi)^2}{I_p}$$

From chapter 4, equation (4-3):

$$\frac{\sigma_{CR}}{} = \frac{E(I_z s^2 + C_w)(m\pi/a)^4 + GJ(m\pi/a)^2 + C_o}{I_p (m\pi/a)^2} \frac{B_o}{B_o^* + B_o}$$

The following is a comparison for a Tee stiffener and a flat bar stiffener which was presented in reference (3). Figure (5-1) from reference (3) shows the geometric dimensions of the Tee and flat bar stiffeners. Table (5-1) shows how equations 21 and 22 of reference (3) and equations (2-2) and (4-3) of this thesis compare with a finite element analysis performed

using a computer program developed and documented at the University of California (reference 12).

| Flat Bar | $(\varepsilon_{CR}/E) \times 10^4$ | | C = 0 |
|---|---|---|---|
| | FEM | EQN(22) | EQN(4-3) |
| m = 1 | 6.44 | 6.42 | 6.28 |
| m = 2 | 7.58 | 7.51 | 7.03 |
| **Tee** | $(\varepsilon_{CR}/E) \times 10^4$ | | C = 0 |
| | FEM | EQN(21) | EQN(2-2) |
| m = 1 | 26.4 | 26.3 | 30.69 |
| m = 2 | 65.9 | 72.6 | 89.4 |

Table (5-1) Comparison with Published Formulae

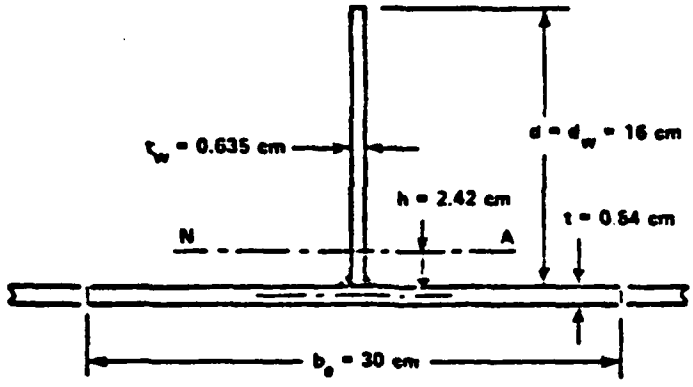


FLAT BAR STIFFENER – a = 100 cm

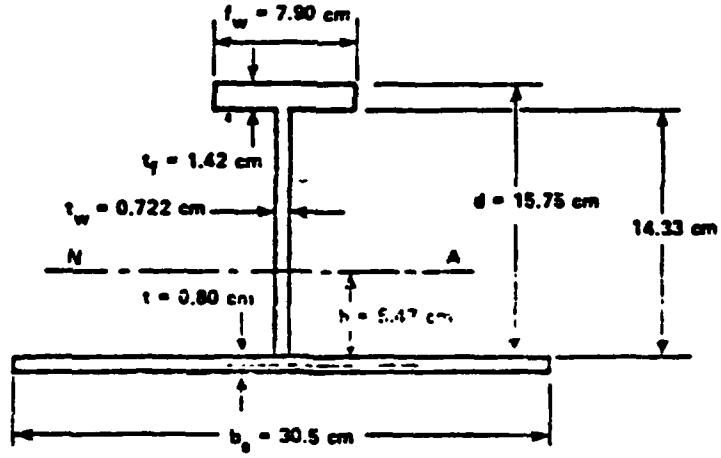


TEE STIFFENER – a = 160 cm

Figure (5-1) Stiffener Geometries for Comparative Solutions

The U.S. Navy has in the past used similar formula as those presented here for the determination of critical buckling stresses. For the critical buckling stress of a Tee stiffener, in the notation of this thesis from reference 13 we have:

$$\sigma_{CR} = \frac{GJ + (m\pi/a)^2 EC_w}{I_p}$$

where here:

$$C_w = f_w d_w^3 t_f^2/12 + d_w^3 t_w$$

$$I_p = d_w t_w^3/3 + d_w f_w t_w^2 + f_w t_f^3$$

This is very similar to those results determined by reference (3), with the exception that the above formula does not account for the rotational restraint provided by the junction of the web and plate. Also $I_p$ is much simplified here and $C_w$, the torsion-bending constant, equates to the quantity $(I_z s^2 + C_w)$ of reference (3) - but also somewhat simplified.

## 5.3 Comparisons with Experimental Results.

Reference (6) provides insight into the torsional buckling process through the experimental results published there. This report describes model tests on the collapse and post failure strength of Tee struts simulating flat bar stiffeners in a stiffened plate. The T struts were subjected to an axial load up to and beyond failure. The geometrical imperfections of the models were also recorded. The researchers of reference (6) (of Det norske Veritas) are to be lauded for the thoroughness and completeness of their report, particularly in the treatment of the experimental data.

Table (5-2) contains the model data pertaining to this analysis for ten experiments of reference (6). Figures (5-2 to 5-11) show the load- deflection curves for these ten experiments. The solid line represents the experimental data. Point A of each of these graphs represents the first yield load point as determined by equation (4-11).

Notice that there is very good correlation between the experimental first yield load point and the results of equation (4-11).

| Model | a | h | $t_w$ | $B_o^*$ | $\sigma_y$ | $\sigma_{CR}$ | $\sigma_u$ |
|---|---|---|---|---|---|---|---|
| 21 | 703 | 87.4 | 4.0 | 1.67E-02 | 256 | 233 | 230 |
| 22 | 703 | 87.3 | 4.0 | 5.6E-03 | 271 | 263 | 246 |
| 23 | 703 | 87.7 | 4.0 | 1.15E-02 | 273 | 257 | 234 |
| 24 | 703 | 87.7 | 4.0 | 6.0E-03 | 271 | 262 | 240 |
| 25 | 703 | 87.7 | 4.0 | 8.0E-03 | 272 | 260 | 230 |
| 26 | 703 | 87.7 | 4.0 | 8.0E-03 | 256 | 244 | 243 |
| 27 | 703 | 87.4 | 4.0 | 6.0E-03 | 266 | 257 | 272 |
| 28 | 703 | 88.0 | 4.0 | 7.99E-03 | 256 | 244 | 241 |
| 29 | 703 | 87.8 | 4.0 | 4.96E-03 | 259 | 252 | 218 |
| 30 | 703 | 88.1 | 4.0 | 1.26E-02 | 271 | 253 | 230 |

Notation:

a - length of model (cm)

h - height of stiffener (cm)

$t_w$ - thickness of stiffener (cm)

$B_o^*$ - angle of rotation (radians)

$\sigma_y$ - yield stress ($N/mm^2$)

$\sigma_{CR}$ - first yield load stress ($N/mm^2$)

$\sigma_u$ - ultimate stress (experimental results) ($N/mm^2$)

Table (5-2) Data of Model Tests

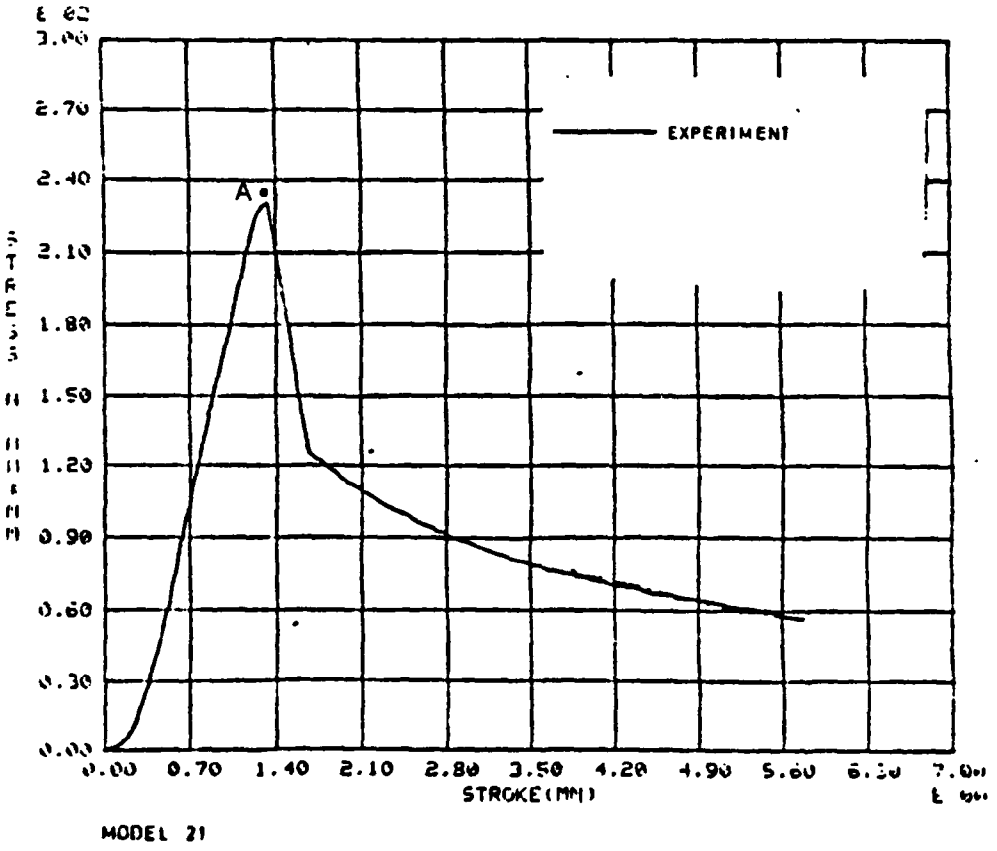


Figure (5-2) Model Test #21 of Reference (6)

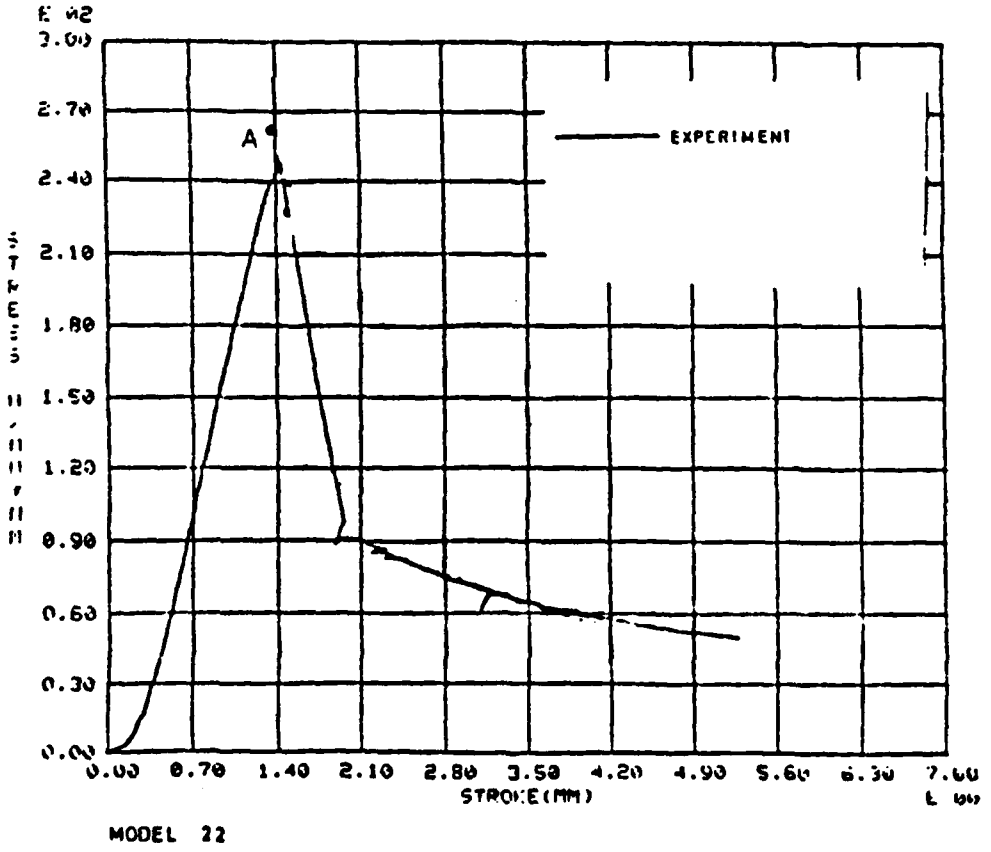


Figure (5-3) Model Test #22 of Reference (6)

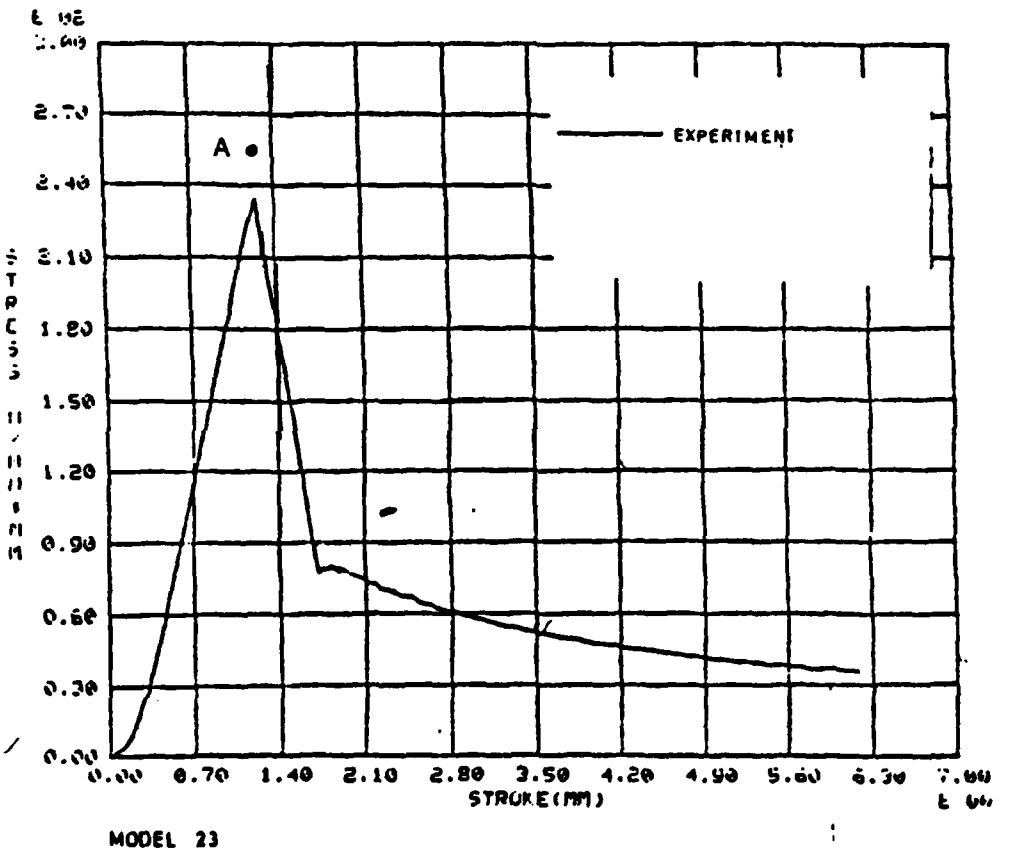


Figure (5-4) Model Test #23 of Reference (6)

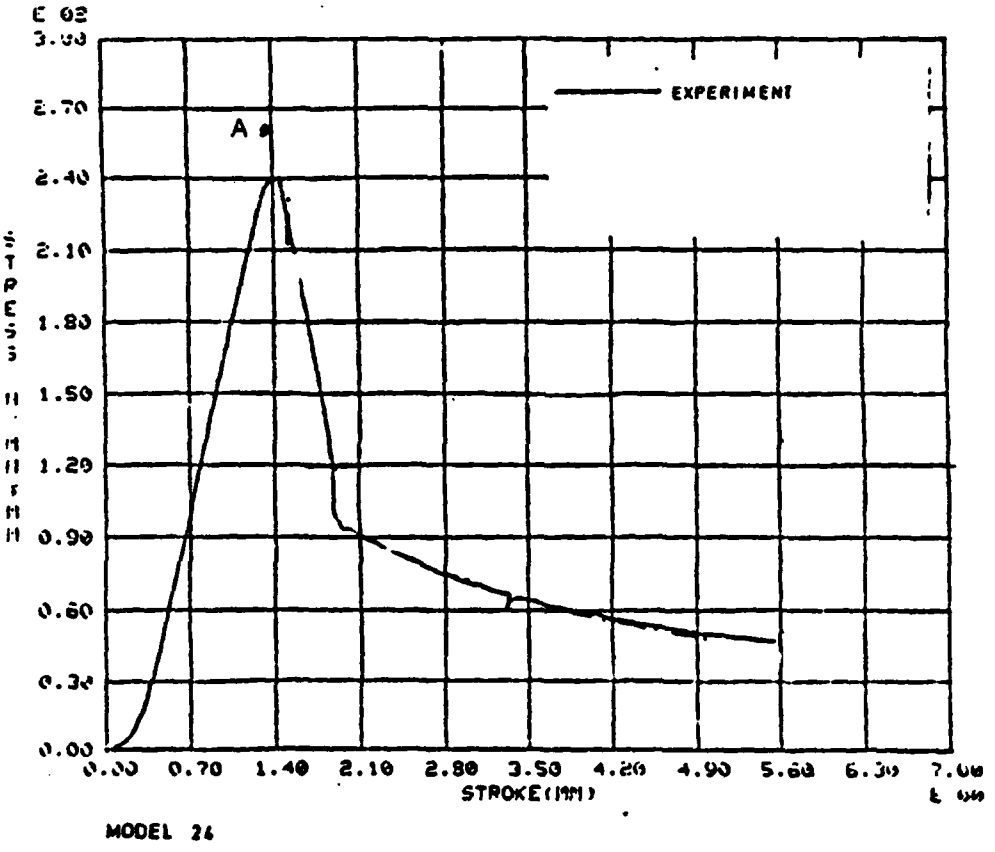


Figure (5-5) Model Test #24 of Reference (6)

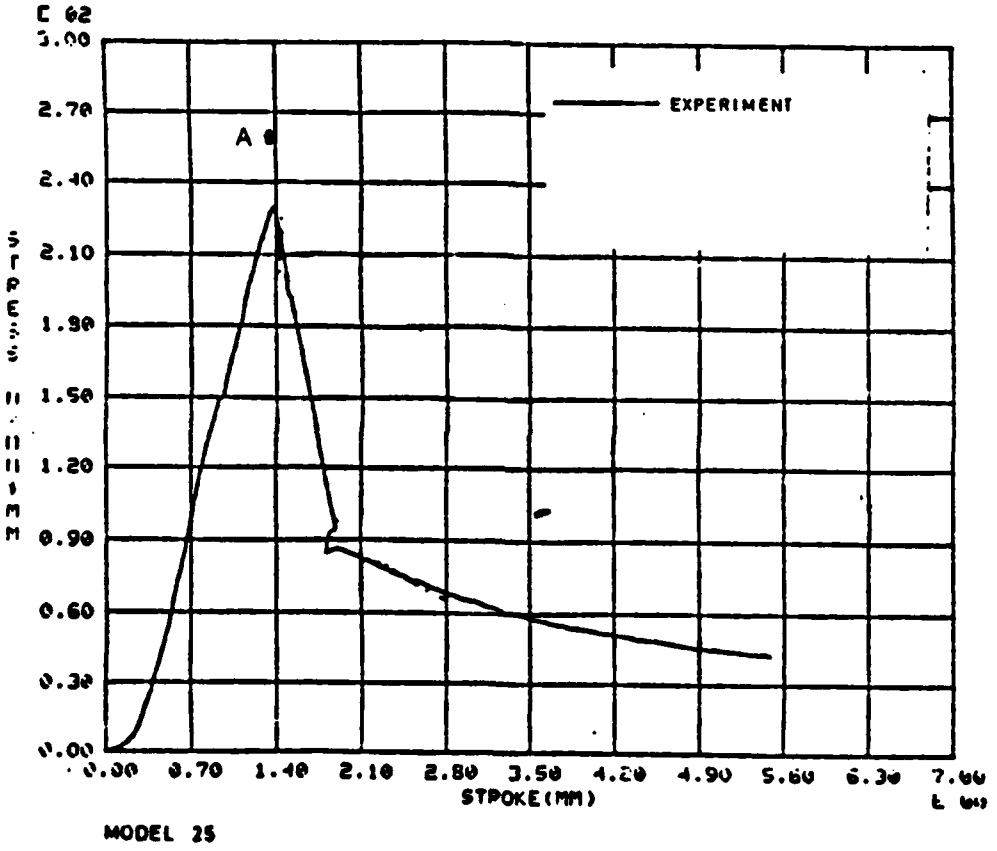


Figure (5-6) Model Test #25 of Reference (6)

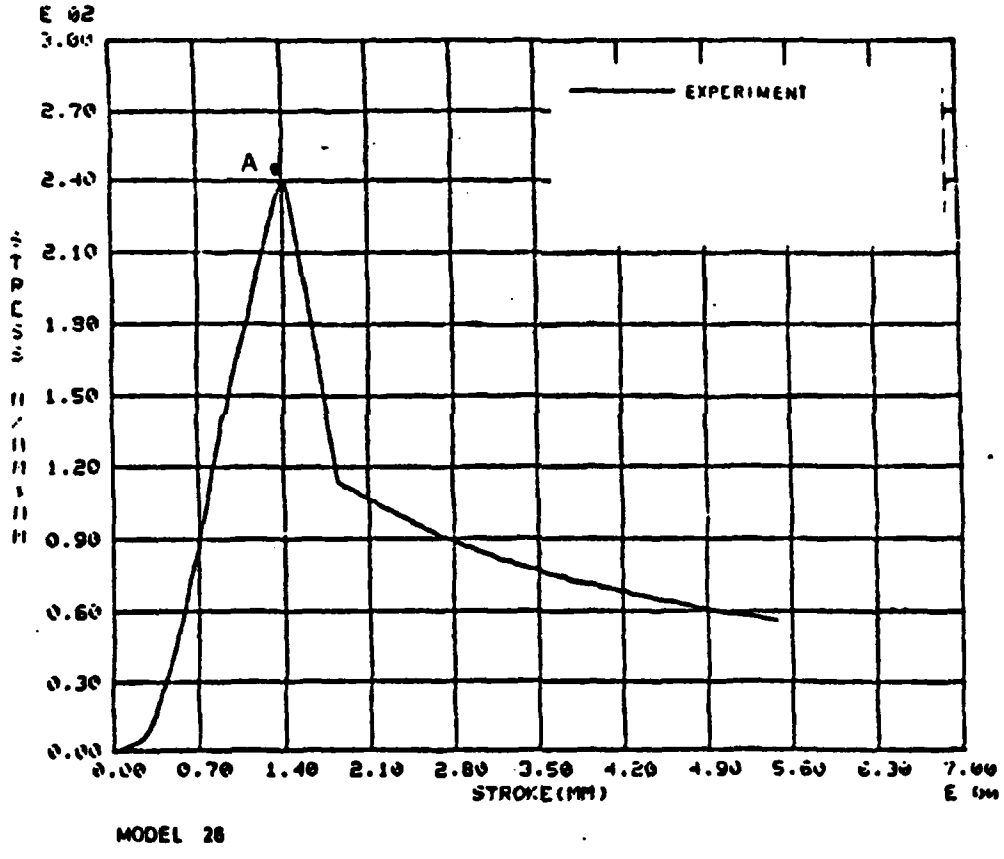


Figure (5-7) Model Test #26 of Reference (6)

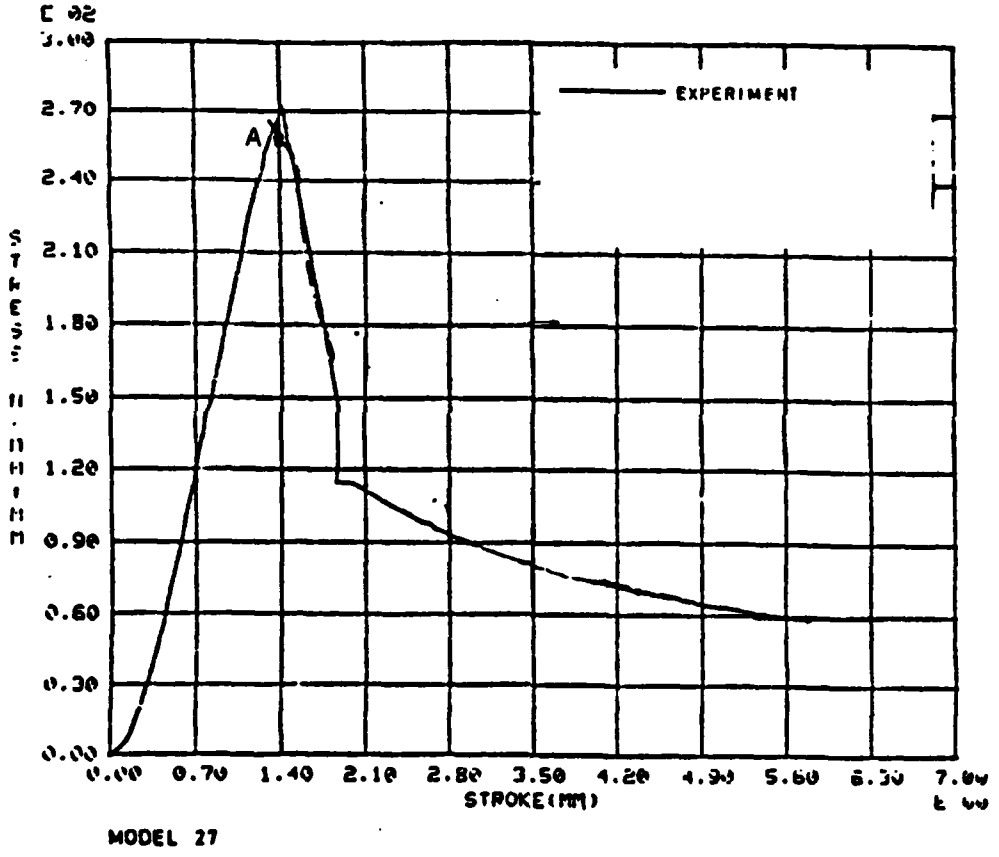


Figure (5-8) Model Test #27 of Reference (6)

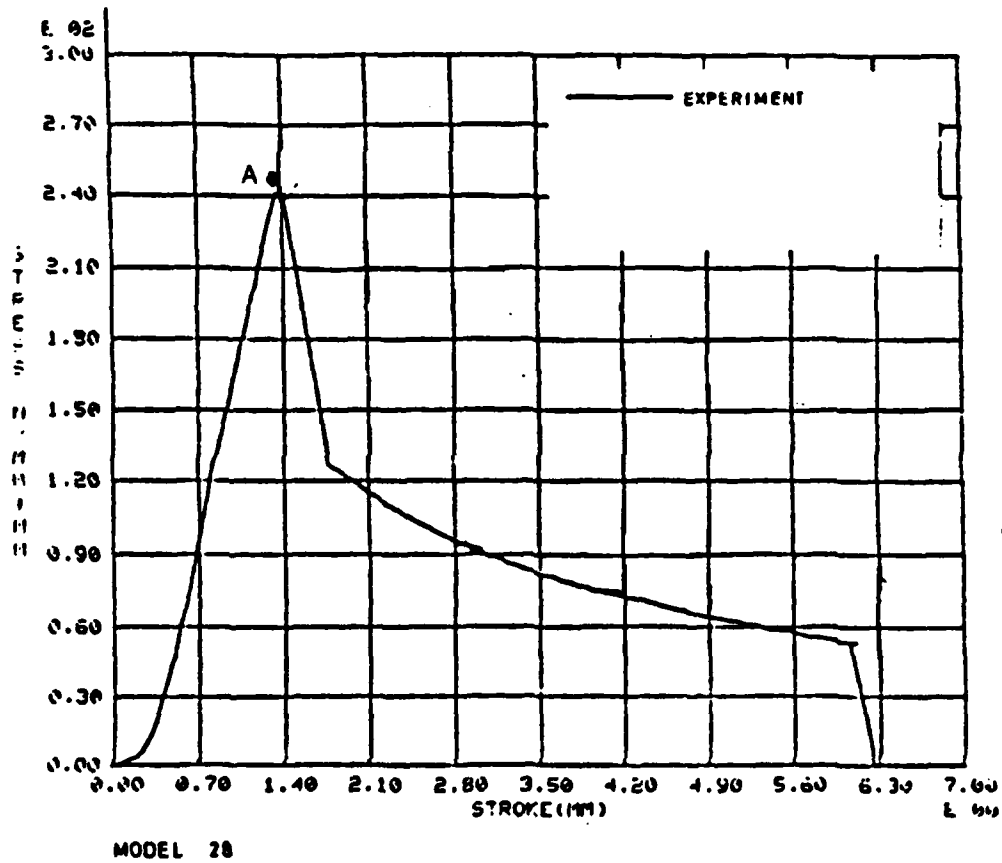


Figure (5-9) Model Test #28 of Reference (6)

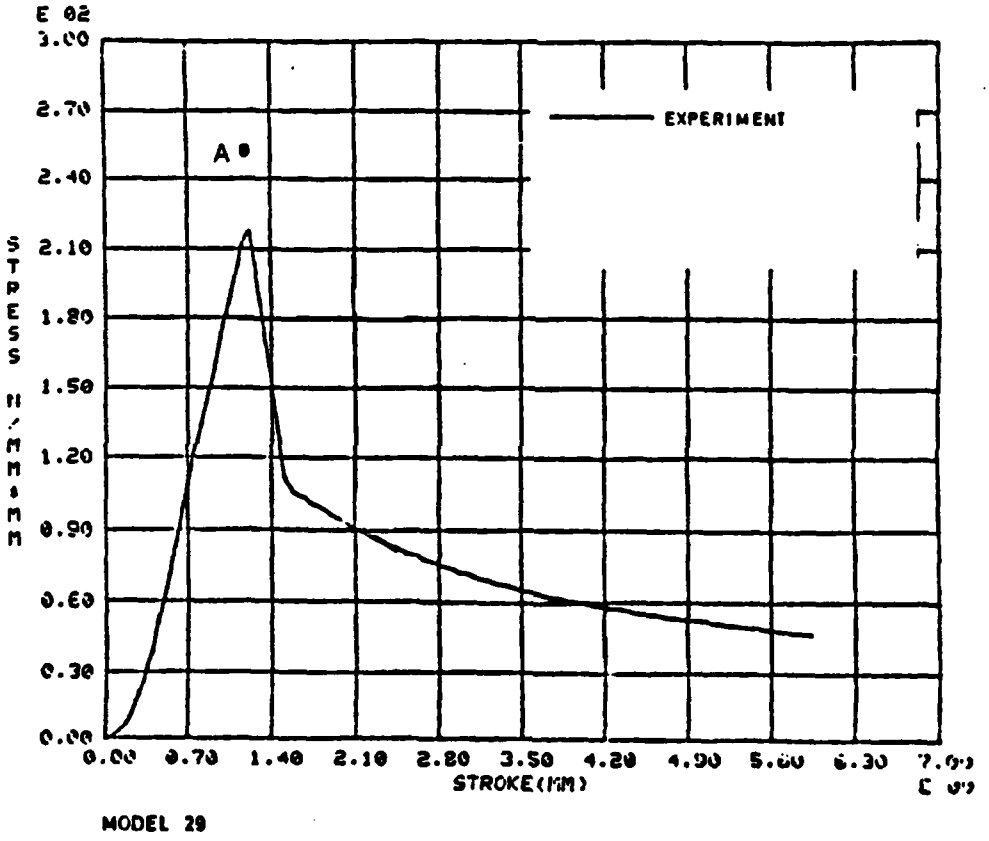


Figure (5-10) Model Test #29 of Reference (6)

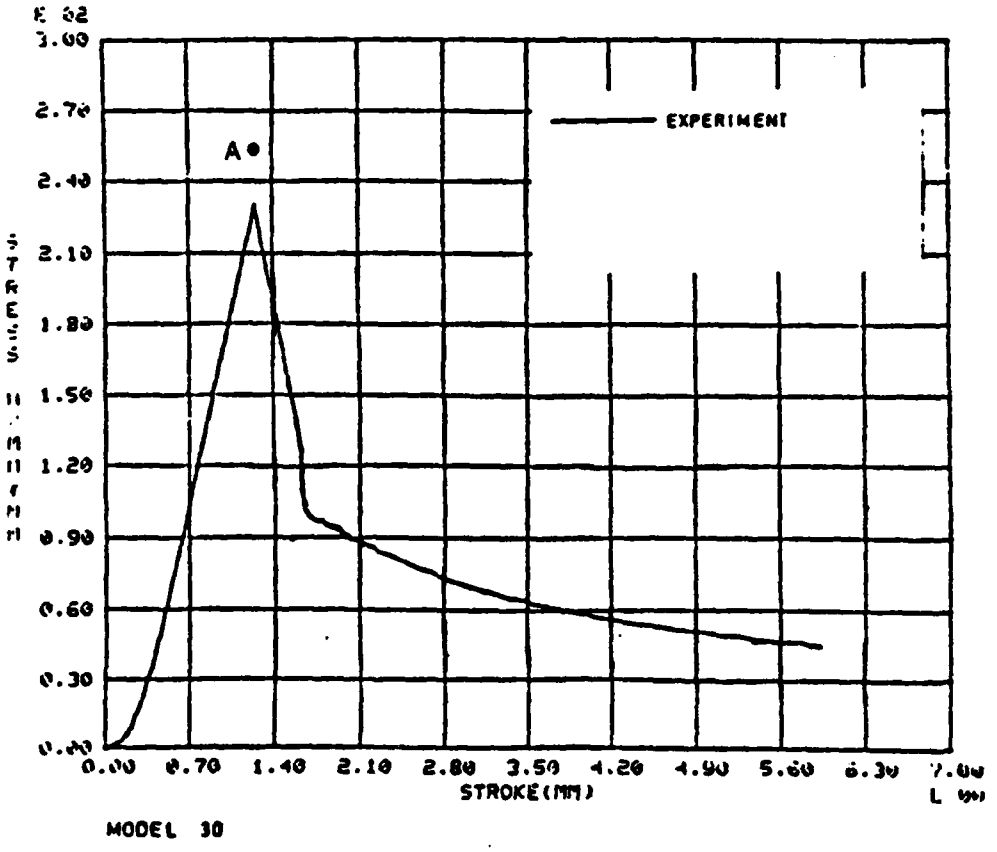


Figure (5-11) Model Test #30 of Reference (6)

# 6. CONCLUSIONS

This thesis utilized a design approach to tackle the problem of torsional buckling of stiffeners with a good deal of success. Integrated into all phases of this analysis was a consideration of the geometric imperfections of the stiffener - both Tee and flat bar. These structural members were analyzed as simplified sections and the Perry-Robertson approach used in other areas of engineering was successfully applied here.

Chapter 5 showed that the derived results of this thesis reduced to currently published formulae for the case of the perfect stiffener. The contribution of this thesis is that the initial imperfections were taken into consideration, using a simple design approach, in the derivation of the results presented here.

Also shown in chapter 5 was a generally good correlation between results of this thesis and axial load tests on flat bar stiffeners. Comparison of the Tee stiffener formula with experimental data, which measures and reports initial imperfections, needs to be performed. Also, comparisons should be made with other tests on flat bar stiffeners in more dimensional ranges to determine the range of validity for the results derived here.

Further work needs to be done in this area. Specifically, determination of the critical buckling stress and first yield load due to lateral loadings. Also, a simplified method of handling the mode interactions of combined lateral and axial loadings is needed. In addition, it is an asset to understand from the work reported in references (6) and (15) that the falling path of the load-deflection curve (figure 6-1) is represented by the tripping mechanism which is not covered in this analysis.

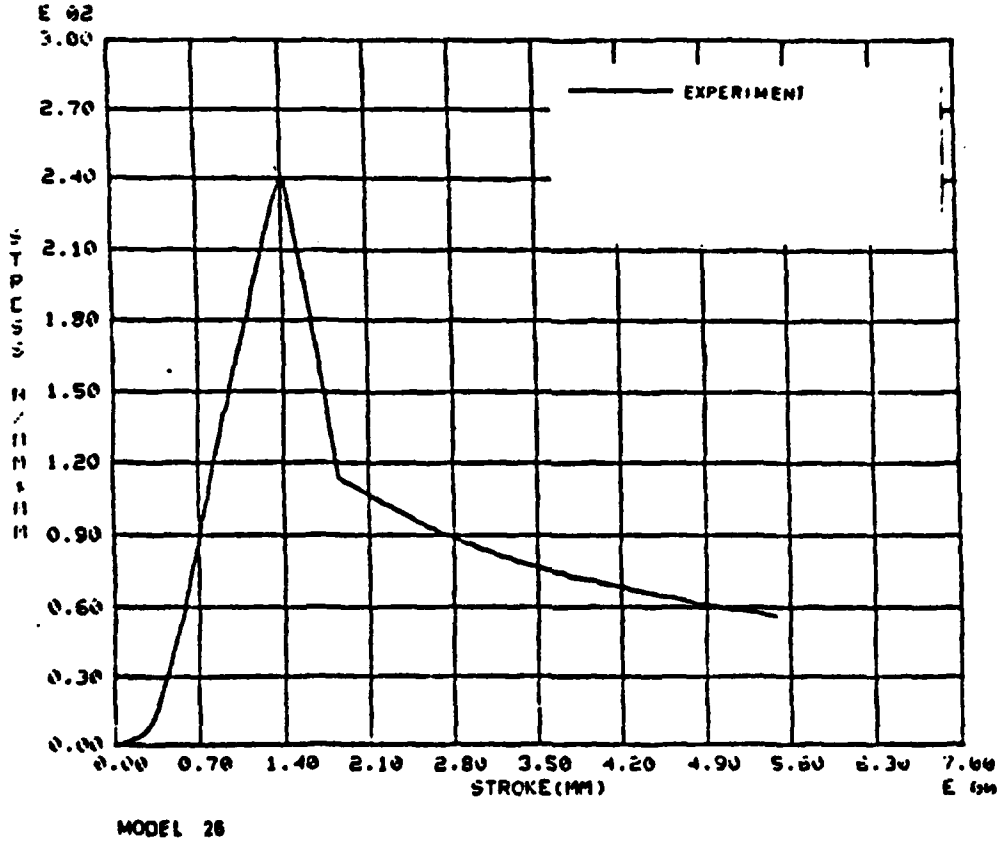


Figure (6-1) Experimental Load Deflection Curve

REFERENCES


(1) Timoshenko S., J. Gere. "Theory of Elastic Stability" 2nd ed., 1961.

(2) 13.122 Course Notes, MIT 1983.

(3) Adamchak, John C., "Design Equations for Tripping of Stiffeners Under Inplane and Lateral Loads" David Talor Naval Ship Research and Development Center, Bethesda, Md., 1979.

(4) ECCS "Second International Colloquium on Stability, Introductory Report", 1977.

(5) Ugural, A.C. "Stresses in Plates and Shells" McGraw-Hill Book Co., 1981.

(6) Carlsen, C.A., W.J Shao, S. Fredheim. "Experimental and Theoretical Analysis of Post Buckling Strength of Flatbar Stiffeners Subjected to Tripping. Det norske Veritas Research Division, Report No 80-0149. 1980.

(7) Atsuta, T, W.F. Chen. "Theory of Beam-Columns" McGraw-Hill Book Co., 1976.

(8) "Data Design Sheet DDS100-4, Strength of Structural Members", Department of the Navy, Naval Ship Engineering Center (Aug 1969).

(9) Perry, J. and W.E. Ayrton. "On Struts" Engineer vol. 62 pp. 464-465, 513-515.

(10) "Rules for the Design Construction and Inspection of Offshore Structures", App. C Steel Structures, Det norske Veritas, 1977.

(11) "Specifications for the Design, Fabrication and Erection of Structured Steel for Buildings", American Institute of Steel Construction.

(12) Kavlie,D. and R.W.Clough, "A Computer Program for Analysis of Stiffened Plates under Combined Inplane and Lateral Loads", University of California Report UCSESM 71-4, Mar 1971.

(13) "Design Data for Tee Stiffeners", U.S.Navy Bureau of Ships, June 1944.

(14) Robertson, A., "The Strength of Struts", Selected Engineering Papers no. 28 ICE 1925.

(15) Murray,N.W., "Buckling of Stiffened Panels Loaded Axially and in Bending", The Structural Engineer, No.8, Vol. 51, 1973.

END

FILMED